1

Charge Transport Simulations for Organic Semiconductors

Hiroyuki Ishii

University of Tsukuba, Division of Applied Physics, 1-1-1 Tennodai, Tsukuba, Ibaraki, 305-8573, Japan

1.1 Introduction

1.1.1 Historical Approach to Organic Semiconductors

Organic semiconductors have the potential to be used in future electronic devices requiring structural flexibility and large-area coverage that can be fabricated by low-cost printing processes. Ordinary organic materials such as plastics (polyethylene) have primarily been regarded as typical electrical insulators. However, graphite exhibits the high electrical conductivity [1], which has been attributed to their molecular structures, which are made of network planes of the conjugated double bonds of carbon atoms with the π-electrons. There exist some organic molecules that have similar molecular structures, for example, aromatic compounds. Around 1950, Eley [2], Akamatu and Inokuchi [3], and Vartanyan [4] have reported that the phthalocyanines, violanthrones, and cyanine dyes have semiconductive characters, respectively. These characters are attributed to the intermolecular overlapping of the electron clouds of π-electrons in the condensed aromatic rings. These materials were named as *organic semiconductors* [5]. However, in general, these organic semiconductors were still recognized as the insulating materials because resistivity of these organic semiconductors is much higher than that of inorganic semiconductors such as silicon and gallium arsenide. The resistivity ρ is given as

$$\frac{1}{\rho} = nq\mu, \tag{1.1}$$

where n, q, and μ represent the carrier concentration, elementary charge of a carrier, and the electron (hole) mobility, respectively. The high resistivity of the organic materials originates from the low carrier concentration and the low mobility.

The carriers can be chemically doped by using the electron–donor–acceptor complexes. In 1954, Akamatu et al. found that the electron–donor–acceptor complex between perylene and bromine is relatively stable and has very good electrical conductance [6]. In 1973, Ferraris et al. have reported that

Molecular Technology: Energy Innovation, Volume 1, First Edition.
Edited by Hisashi Yamamoto and Takashi Kato.

the complex between the electron donor tetrathiafulvalene (TTF) and the electron acceptor tetracyano-*p*-quinodimethane (TCNQ) has the very high conductivity comparable with the conductivities of metals such as copper [7]. Shirakawa et al. also showed that the organic polymer, polyacetylene, has a remarkably high conductivity at room temperature by chemical doping with iodine in 1977 [8]. These complexes are called organic conductors. The high electrical conductivity accelerated interest in organic conductors, not only because of their huge electrical conductivity but also by the possibility of superconductivity [9].

The multicomponent systems as mentioned above have some disadvantageous properties such as air and thermal instability in general. Therefore, semiconducting single-component organic compounds are likely to be much more suitable for use as molecular devices. From a viewpoint of the electronic device applications, mobility is very important to evaluate the device performance because it characterizes how quickly an electron can move in a semiconductor when an external electric field is applied. In 1960, Kepler [10] and LeBlanc [11] measured the mobility of an organic semiconductor by the time-of-flight (TOF) technique, where the flight time of carriers in a given electric field is determined by observing an arrival time kink in the current that is caused by a pulse-generated unipolar "charge carrier sheet" moving across a plane-parallel slice of a sample. They reported that the anthracenes have the mobility of 0.1–2.0 $cm^2\ V^{-1}\ s^{-1}$ at room temperature and their mobilities increase as the temperature decreases. Friedman theoretically investigated the electrical transport properties of organic crystals using the Boltzmann equation treatment of narrow-band limit in the case of small polaron band motion [12]. Sumi also discussed the change from the band-type mobility of large polarons to the hopping type of small polarons, using the Kubo formula with the adiabatic treatment of lattice vibrations in the single-site approximation [13]. However, the mobility obtained by TOF technique is different from the mobility of actual devices such as field-effect transistors (FETs) because the charge carriers are induced at the interface between the organic semiconductor and the dielectric film by an applied gate voltage. Kudo et al. reported the field-effect phenomena of merocyanine dye films and their field-effect mobilities of 10^{-7}–$10^{-5}\ cm^2\ V^{-1}\ s^{-1}$ estimated from the measurements in 1984 [14]. Then, Koezuka et al. fabricated the actual FET utilizing polythiophene as a semiconducting material and reported the mobility of $10^{-5}\ cm^2\ V^{-1}\ s^{-1}$ [15].

A major industrial breakthrough occurred in the application to electroluminescent (EL) devices. Tang and VanSlyke reported the first organic EL device based on a π-conjugated molecular material in 1987 [16]. After that, typical industrial applications spread to light-emitting diodes (LEDs) [17, 18] and solar cells [19–21]. Recently, organic semiconductors are expected as the future electronic device semiconducting materials requiring structural flexibility and large-area coverage that can be fabricated by low-cost printing processes [22, 23]. However, we have a massive task for the realization of the "printed electronics," for example, increasing the mobility, improvement of the solubility, and thermal durability, suppressing the variations of device characteristics, decreasing the threshold voltage, and so on.

Although π-conjugated polymers with aromatic backbones have been widely investigated as soluble organic semiconductors, further improvement of mobility of polymer semiconductors has disadvantages owing to the statistical distribution of molecular size and structural defects caused by mislinkage of monomers, which act as carrier traps in the semiconducting channel. Therefore, small molecular materials, such as pentacene (see Figure 1.1a), have advantages in terms of their well-defined crystal structure and ease of purification. At first, the organic transistors were fabricated utilizing the organic polycrystals. For example, the field-effect mobility of polycrystal thin-film transistors (TFTs) increases in proportion to the grain size [63, 64]. The mobility in the polycrystals is mainly limited by the grain boundaries, and the typical highest value is generally below 1.0 $cm^2\ V^{-1}\ s^{-1}$ at room temperature. The temperature dependence with a thermally activated behavior indicates that the incoherent hopping process of spatially localized carriers between trap sites is dominated in the polycrystals [26]. In such a low-mobility regime, the charge transport mechanism has been investigated theoretically using the Marcus theory [65, 66] based on the small polaron model [67].

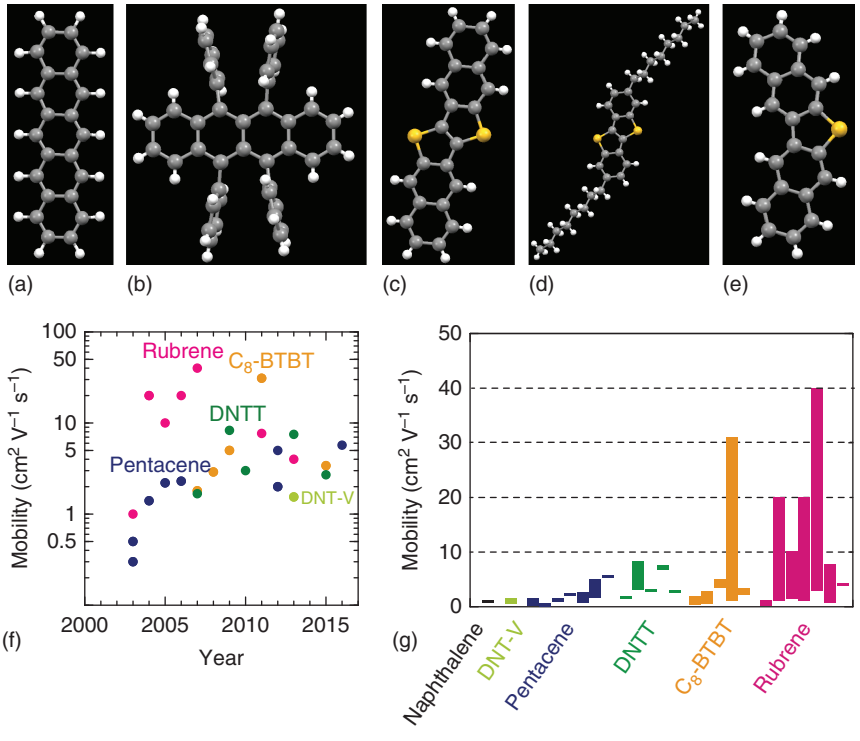

Figure 1.1 Molecular structures of (a) pentacene, (b) rubrene, (c) DNTT, (d) C_8-BTBT, and (e) DNT-V. (f) Annual change of the highest hole mobilities of different organic single-crystal field-effect transistors in the literature, and (g) the distribution of the reported mobilities for naphthalene [24], DNT-V [25], pentacene [26–35], DNTT [36–41], C_8-BTBT [42–49], and rubrene [29, 31], [50–62].

1.1.2 Recent Progress and Requirements to Computational "Molecular Technology"

Recent rapid progress in technology enables us to fabricate the very pure rubrene single-crystal FETs (see Figure 1.1b) with the high carrier mobility up to 40 $cm^2\ V^{-1}\ s^{-1}$ at room temperature [60], which exceeds the mobility of amorphous silicon [68]. The high mobility attributes the exclusion of trap sites such as grain boundary in organic semiconductors. The mobility monotonically decreases with increasing temperature, $\mu \propto T^{-n}$ [54]. The power-law temperature dependence is a typical characteristic of coherent band transport by spatially extended carriers, which is scattered by the molecular vibrations (phonons). The rubrene single crystals obtained by the physical vapor deposition method show the excellent high mobilities at room temperature, but their poor solubility is a serious problem for the printed electronics. In 2006, Takimiya et al. reported solution-processable organic semiconductors based on [1]benzothieno[3,2-*b*][1]benzothiophene (BTBT) core [69] and dinaphtho[2,3-*b*:2′,3′-*f*]thieno[3,2-*b*]thiophene (DNTT) core [36] with high mobility and stability, as shown in Figure 1.1c,d. Moreover, Okamoto et al. reported a new candidate semiconducting material based on V-shaped dinaphtho[2,3-*b*:2′,3′-*d*]thiophene (DNT-V) core (Figure 1.1e), with high mobility, solubility, and thermal durability [25]. Figure 1.1f,g shows annual change of the highest hole mobilities of different organic single-crystal FETs in the literature, and the distribution of the reported mobilities for naphthalene [24], DNT-V [25], pentacene [26–35], DNTT [36–41], C_8-BTBT [42–49], and rubrene [29, 31, 50–62].

As shown above, new organic semiconductors with higher mobilities have been required. It is a very important and an urgent issue for us to establish the method and system for finding new organic semiconductors with high mobility from among various kinds of the candidate materials. Computer simulation to predict the mobility of candidate organic semiconductors becomes a powerful tool to accelerate the material development.

1.2 Theoretical Description of Charge Transport in Organic Semiconductors

As shown in Figure 1.2a, different from covalent crystals such as silicon, organic semiconductors are formed with van der Waals interactions between molecules [70]. The very weak interactions give the organic semiconductors the property of mechanical flexibility and the solubility. Charge carriers in organic semiconductors strongly couple with the molecular vibrations, namely, phonons. The total Hamiltonian consists of that for the electron $\hat{H}_{\mathrm{e}}$, the phonon $\hat{H}_{\mathrm{ph}}$, and the interaction $\hat{H}_{\mathrm{e-ph}}$,

$$\hat{H} = \hat{H}_{\mathrm{e}} + \hat{H}_{\mathrm{ph}} + \hat{H}_{\mathrm{e-ph}}. \tag{1.2}$$

The general expression can be given on the basis of molecular orbitals and the eigenfunctions of phonon as follows:

$$\hat{H}_{\mathrm{e}} = \sum_{m,n} h^0_{mn} \hat{a}^{\dagger}_m \hat{a}_n, \tag{1.3}$$

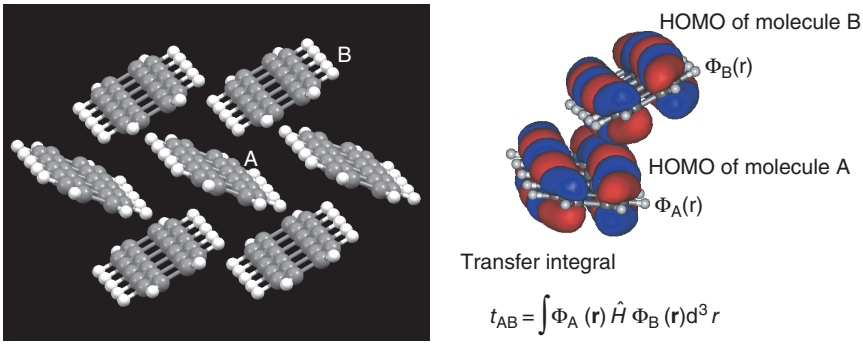

Figure 1.2 (a) Structure of a single crystal of pentacene. (b) HOMOs of the molecules labeled A and B in (a). The transfer integral between molecules t_{AB} is defined as the off-diagonal elements of the Hamiltonian matrix $\hat{H}$ on the molecular orbital basis set.

$$\hat{H}_{\text{ph}} = \sum_{\lambda,\mathbf{q}} \hbar\omega_{\lambda\mathbf{q}} \left(\hat{b}^{\dagger}_{\lambda\mathbf{q}} \hat{b}_{\lambda\mathbf{q}} + \frac{1}{2} \right), \tag{1.4}$$

$$\hat{H}_{\text{e-ph}} = \sum_{m,n} \sum_{\lambda,\mathbf{q}} \hbar\omega_{\lambda\mathbf{q}} g^{\lambda\mathbf{q}}_{mn} \hat{a}^{\dagger}_{m} \hat{a}_{n} (\hat{b}^{\dagger}_{\lambda\mathbf{q}} + \hat{b}_{\lambda-\mathbf{q}}), \tag{1.5}$$

where $\hat{a}^{\dagger}_{n}$ and $\hat{b}^{\dagger}_{\lambda\mathbf{q}}$ represent the creation operator of electron at the nth orbital and the correlation operator of phonon with mode λ, wave-vector $\mathbf{q}$, and the vibration frequency $\omega_{\lambda\mathbf{q}}$. Here, $h^{0}_{mn(m\neq n)}$ and h^{0}_{nn} are the transfer integral t^{0}_{mn} between nth and mth molecular orbitals and the orbital energy ε^{0}_{n} at the equilibrium position, respectively. As an example, the highest occupied molecular orbitals (HOMOs) of the pentacene molecules are shown in Figure 1.2b [70]. The dimensionless electron–phonon coupling constant is defined by [71, 72]

$$g^{\lambda\mathbf{q}}_{nm} \equiv \sum_{k,s} \sqrt{\frac{1}{2\hbar M N \omega^{3}_{\lambda\mathbf{q}}}} e^{i\mathbf{q}\mathbf{R}_{k}} \left(\frac{\partial h_{nm}}{\partial \mathbf{R}_{ks}} \right) \mathbf{e}^{\lambda\mathbf{q}}_{s}, \tag{1.6}$$

where $\mathbf{e}^{\lambda\mathbf{q}}_{s}$ is the phonon eigenvector representing the direction of displacement of sth atom. M and N represent the mass of a single molecule and the number of unit cells. The position of sth atom in kth unit cell is given by $\mathbf{R}_{ks} = \mathbf{r}_{s} + \mathbf{R}_{k}$, where the relative position of sth atom in the unit cell is represented by $\mathbf{r}_{s}$, and $\mathbf{R}_{k}$ is the position vector of kth unit cell. The change in transfer integral due to molecular vibration ($\partial h/\partial \mathbf{R}$) is an intrinsic meaning of the electron–phonon interaction.

The relation between the mobility μ and the diffusion coefficient D is well used in theoretical studies of transport of carrier with charge q in organic semiconductors and known as the Einstein relation

$$\mu = \frac{qD}{k_{\text{B}}T}, \tag{1.7}$$

where $k_{\text{B}}T$ is the thermal energy defined as the product of the Boltzmann constant and the temperature. The problem remained is how we obtain the diffusion coefficient from the general Hamiltonian of Eqs. (1.3)–(1.5).

1.2.1 Incoherent Hopping Transport Model

The semiclassical Marcus theory [65, 66] based on the small polaron model [67] describes the hopping motion of charge carriers that are self-trapped in a single molecule by their induced intramolecular deformations. The schematic picture of hopping motion is shown in Figure 1.3a [70]. Before injection of a charge carrier, all molecules in the organic semiconductor are in the neutral state. As shown in Figure 1.3b, when a charge carrier is injected into a single molecule, the state is changed from the most stable neutral state (i) to the charged state (ii). Then, the state (ii) relaxes into the most stable charged state (iii) by their induced intramolecular distortion. If we assume that the transfer integrals are much smaller than the magnitude of electron–phonon couplings, the hopping rate to neighboring jth molecule can be calculated using the perturbation theory and takes the following thermally activated form:

$$\frac{1}{\tau_j^{\mathrm{hop}}} = \frac{|t_j^0|^2}{\hbar}\sqrt{\frac{\pi}{\lambda k_{\mathrm{B}} T}}\mathrm{e}^{-\frac{\lambda}{4k_{\mathrm{B}}T}}, \tag{1.8}$$

where t_j^0 is the transfer integral at the equilibrium position. The quantity $\lambda \equiv \lambda^{(1)} + \lambda^{(2)}$ is the reorganization energy. Here, two components $\lambda^{(1)}$ and $\lambda^{(2)}$ correspond to going into a charged state and returning to a neutral state as shown in Figure 1.3b.

Moreover, we assume that the quantum coherence is lost after each hopping event, the diffusion coefficient is given by

$$D^{\mathrm{hop}} = \sum_j a_j^2 \frac{P_j}{\tau_j^{\mathrm{hop}}}, \tag{1.9}$$

where a_j represents the intermolecular distance and the hopping probability is defined by $P_j \equiv (\tau_j^{\mathrm{hop}})^{-1}/\sum_k (\tau_k^{\mathrm{hop}})^{-1}$. Finally, we can obtain the thermally activated form of hopping mobility using the Einstein relation of Eq. (1.7). In the case of simple one-dimensional molecular crystals with the intermolecular transfer integral t and the intermolecular distance a, the hopping mobility is written by

$$\mu^{\mathrm{hop}} = \frac{1}{2}\frac{a^2|t|^2}{\hbar}\frac{q}{k_{\mathrm{B}}T}\sqrt{\frac{\pi}{\lambda k_{\mathrm{B}} T}}\mathrm{e}^{-\frac{\lambda}{4k_{\mathrm{B}}T}}. \tag{1.10}$$

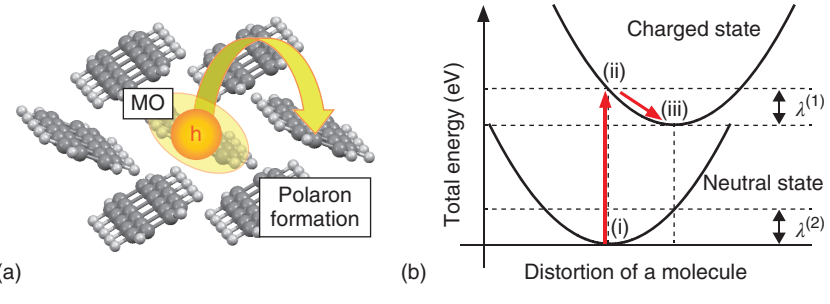

Figure 1.3 (a) Schematic picture of the hopping transport. Charge carrier localized at a molecule moves to the neighboring molecules by the thermally activated hopping process. (b) Potential energy surface for the neutral state and the charged state of the single molecule.

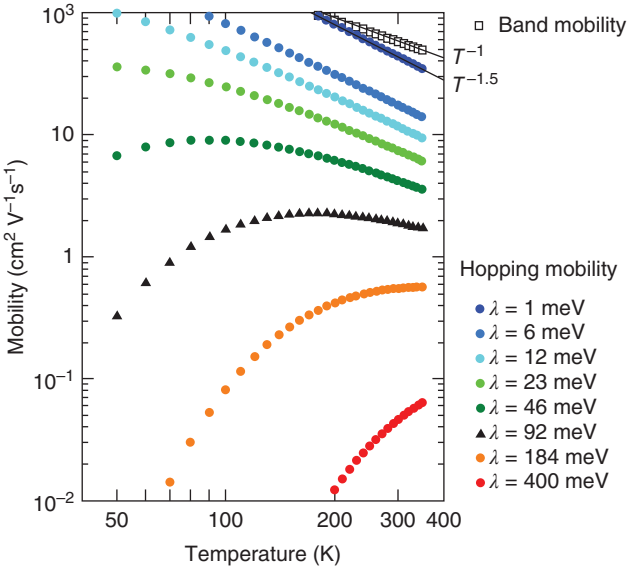

Figure 1.4 Temperature-dependent behavior of the hopping and band mobilities of pentacene single crystal with the transfer integrals between adjacent molecules are 43.6, 71.5, and −111.3 meV [73]. The reorganization energy of a pentacene molecule is λ =92 meV and the calculated hopping mobility is shown by the black triangles. For the reference, the hopping mobilities are calculated for the several reorganization energies from 1 to 400 meV. The calculated band mobility is represented by the white squares. *Source*: Ishii et al. 2017 [73]. Reproduced with permission of American Physical Society.

Figure 1.4 shows the temperature-dependent behavior of the hopping mobility of the two-dimensional pentacene single crystal by the black triangles. The calculated intermolecular transfer integrals 43.6, 71.5, and −111.3 meV [73] are comparable to the reorganization energy $\lambda = 92$ meV. Interestingly, the calculated hopping mobility of pentacene single crystal exhibits temperature-independent mobility around room temperature with a mobility of ~ 1 cm^2 V^{-1} s^{-1}. The calculated results seem to well explain the experimentally observed temperature-independent mobility [27]. However, the Marcus theory is generally applicable for $t \ll \lambda$. It indicates that we should not employ the Marcus theory for the analysis of charge transport of high-mobility organic semiconductors.

1.2.2 Coherent Band Transport Model

The band transport model starts from the solution of the electronic problem in an unperturbed, perfect lattice (perfect periodicity). In this limit, the electrons form the Bloch waves identified by a well-defined momentum $\mathbf{k}$ and the energy band dispersion $E(\mathbf{k})$. As an example, the HOMO band dispersion calculated by the density functional theory (DFT) using the plane-wave basis set is shown in Figure 1.5b [70]. The existence of HOMO band dispersion of pentacene crystal [74–77] is experimentally demonstrated using angle-resolved photoelectron spectroscopy (ARPES). Quantum mechanics tells us that a charge carrier having the effective mass $\mathbf{m}(\mathbf{k})$ propagates at the group velocity $\mathbf{v}(\mathbf{k})$ without

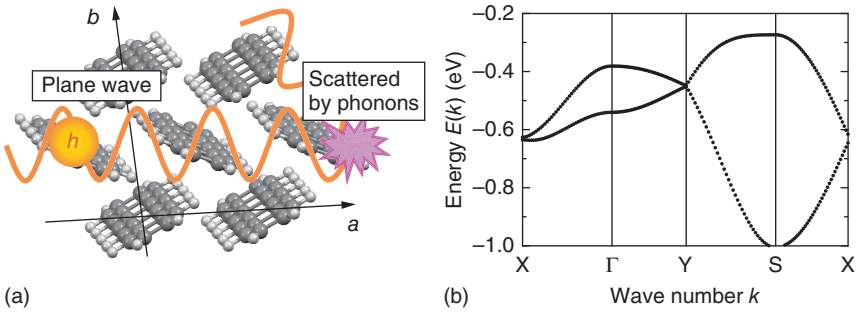

Figure 1.5 (a) Schematic picture of the band transport. Extended charge carriers are described by the Bloch states with the wave-vector **k** and scattered by the molecular vibrations (phonons). (b) HOMO bands obtained from DFT using the plane-wave basis set with symmetry points of Γ(0, 0, 0), X(1/2, 0, 0), Y(0, 1/2, 0), and S(1/2, 1/2, 0). The Fermi energy is located at $E = 0$ eV.

any scattering in the perfect lattice. The effective mass and the group velocity are obtained from the band dispersion as follows: $\mathbf{v}(\mathbf{k}) \equiv \partial E(\mathbf{k})/\hbar\partial\mathbf{k}$ and $\mathbf{m}(\mathbf{k}) \equiv (\partial^2 E(\mathbf{k})/\hbar^2\partial\mathbf{k}^2)^{-1}$. However, as shown in Figure 1.5a, even if the perfect single crystal can be made, the molecular vibrations disturb the periodicity and become a dominant origin of electric resistance at room temperature. Scattering of the Bloch states by the molecular vibrations is included as a perturbation in the band transport model. The momentum relaxation time (scattering time) of τ^{band} is given by Fermi's golden rule,

$$\frac{1}{\tau^{\text{band}}(\mathbf{k})} = \frac{2\pi}{\hbar}\sum_{\mathbf{k}'}\sum_{\lambda\mathbf{q}} |\langle\mathbf{k}'|\hat{H}|\mathbf{k}\rangle|^2 \times \delta(E(\mathbf{k}') - E(\mathbf{k}) \pm \hbar\omega_{\lambda\mathbf{q}})(1 - \cos\theta_{\mathbf{k}'\mathbf{k}}), \tag{1.11}$$

where $|\mathbf{k}\rangle$ represents the eigenfunction of $\hat{H}_e$ with the eigenenergy $E(\mathbf{k})$ in the momentum representation, and $\theta_{\mathbf{k}'\mathbf{k}}$ is the angle between $\mathbf{k}$ and $\mathbf{k}'$. In the acoustic deformation potential model for two-dimensional transport [78], the relaxation time can be calculated as

$$\frac{1}{\tau^{\text{band}}(T)} = \frac{\varepsilon_{\text{ac}}^2 m_{\text{d}} k_{\text{B}} T}{\hbar^3 B L_{\text{eff}}}. \tag{1.12}$$

Here, ε_{ac} is the acoustic deformation potential defined by $\varepsilon_{\text{ac}} \equiv \Omega \text{d}E_{\text{hbm}}/\text{d}V$, where E_{hbm} represents the value to the HOMO band maximum. The acoustic deformation potential should be the quantity as a function of the electron–phonon coupling constant g of Eq. (1.6). B is the elastic modulus, L_{eff} is the effective channel width of carrier confinement layer, and m_{d} is the density of states mass, which is equal to $\sqrt{m_a m_b}$. m_a and m_b represent the effective mass at the HOMO band maximum along a and b axes, respectively.

Different from the hopping model, the diffusion coefficient along x axis is defined as $D_x^{\text{band}} \equiv \int_0^{+\infty} v_x(s)v_x(0)\text{d}s$, using the velocity correlation functions, where $v_x(s)$ is the x component of the group velocity $\mathbf{v}$ at time s. When the velocity correlation is disappeared by the molecular vibrations, the diffusion

coefficient is calculated as

$$\begin{aligned} D_x^{\text{band}} &= \int_0^{+\infty} v_x^2 \exp\left(\frac{-s}{\tau^{\text{band}}}\right) \mathrm{d}s, \\ &= v_x^2 \tau^{\text{band}}. \end{aligned} \tag{1.13}$$

The band mobility is obtained from the Einstein relation of Eq. (1.7) as follows:

$$\begin{aligned} \mu_x^{\text{band}} &= \frac{q}{k_{\text{B}}T} v_x^2 \tau^{\text{band}}, \\ &= \frac{q\tau^{\text{band}}(T)}{m_x}, \\ &= \frac{q}{m_x} \frac{\hbar^3 B L_{\text{eff}}}{\varepsilon_{ac}^2 m_{\text{d}} k_{\text{B}} T}. \end{aligned} \tag{1.14}$$

Here, the relation between the kinetic energy and the temperature, $\frac{3}{2}mv^2 = \frac{3}{2}k_{\text{B}}T$, has been used. The calculated band mobility decreases with increasing temperature, according to $\mu \propto T^{-1}$ shown by the white squares in Figure 1.4. Such power-law temperature dependence is a typical character of coherent band transport and has been observed in some experiments for organic single crystals with high mobility [24, 45, 54, 55]. Moreover, recent experiments of Hall effects on the organic FETs provide us with an evidence of possible coherent charge transport in the organic semiconductors [55, 56, 59, 79]. On the other hand, a difficult problem is still remained in the coherent band picture. That is, the estimated mean free path is comparable to or shorter than the distance between adjacent molecules [27], which implies a breakdown of the coherent band transport.

1.2.3 Coherent Polaron Transport Model

Some experiments reported that the width of HOMO bands observed by the ARPES is narrowing with increasing temperature [76, 77]. This phenomenon is known as the band narrowing and can be rationalized by means of the concept of polaron, as described in the following. When there exist the electron–phonon interactions, the bare electrons get dressed by phonons (molecular vibrations) and form quasiparticles called polarons. The charge carriers have to carry the phonon cloud as well, which always accompanies the carrier. With increasing temperature, the effective mass of polaron becomes larger since much more phonons are available that coupled to the charge carrier.

Hannewald et al. have derived analytically the total Hamiltonian of coherent polaron $\tilde{H}$ from $\hat{H}$ of Eq. (1.2), using the method of the Lang-Firsov canonical transformation [71, 72, 80],

$$\tilde{H} = \mathrm{e}^{\hat{S}} \hat{H} \mathrm{e}^{\hat{S}^\dagger}, \tag{1.15}$$

$$\simeq \sum_{m,n} \tilde{t}_{mn} \hat{a}_m^\dagger \hat{a}_n + \hat{H}_{\text{ph}}, \tag{1.16}$$

where $\hat{S} \equiv \sum_{m,n} \hat{C}_{mn} \hat{a}_m^\dagger \hat{a}_n$ and $\hat{C}_{mn} \equiv \sum_{\lambda,\mathbf{q}} g_{mn}^{\lambda\mathbf{q}} (\hat{b}_{\lambda\mathbf{q}}^\dagger - \hat{b}_{\lambda-\mathbf{q}})$. To get Eq. (1.16) from Eq. (1.15), they have assumed that the electron–intramolecular vibration coupling is much stronger than the electron–intermolecular vibration coupling ($|g_{mm}| \gg |g_{mn}|$) and the coherent part is dominant than the incoherent hopping

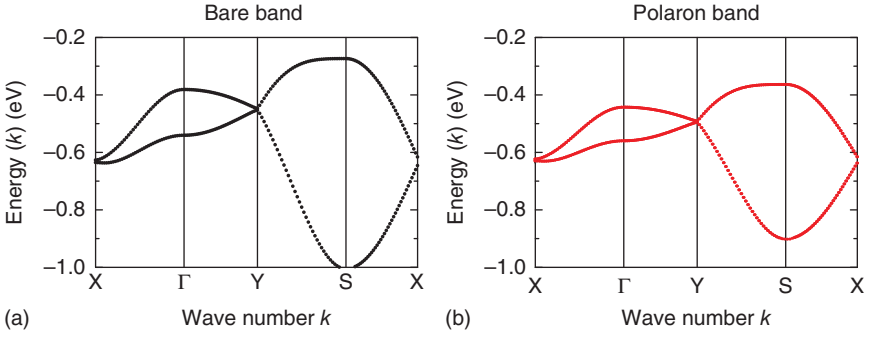

Figure 1.6 (a) HOMO band dispersion of bare electron of the pentacene single crystal. (b) Schematic picture of band narrowing by polaron formation.

part described by the Marcus theory. The transfer integrals of coherent polaron $\tilde{t}$ are expressed using the bare transfer integral t^0, the electron–phonon couplings g and the number of phonons n as follows:

$$\tilde{t}_{mn} \simeq t^0_{mn} \exp\left\{ -\sum_{\lambda,\mathbf{q}} \left(n_{\lambda\mathbf{q}} + \frac{1}{2} \right) |g^{\lambda\mathbf{q}}_{mm} - g^{\lambda\mathbf{q}}_{nn}|^2 \right\}, \tag{1.17}$$

where $n_{\lambda\mathbf{q}} = (\exp(\hbar\omega_{\lambda\mathbf{q}}/k_B T) - 1)^{-1}$. The band narrowing is included in this expression because $\tilde{t}$ is always smaller than t^0. The schematic pictures of HOMO band dispersion for bare electrons and for polarons are shown in Figure 1.6a,b, respectively.

In analogy with the band mobility of Eq. (1.14), the coherent polaron mobility is obtained using the effective mass of polaron band,

$$\mu_x^{\text{polaron}} = \frac{q\tau}{\tilde{m}_x(T)}. \tag{1.18}$$

Here, τ is the scattering time by static disorders such as impurities and defects. Although the temperature dependence of polaron mobility exhibits the power-law behavior around room temperature, different from the band mobility, the effective mass of polaron, not the scattering time τ, decides the temperature dependence of mobility.

Band narrowing is a prominent feature of the polaron model. However, as already discussed in Section 1.2.1, the polaron concept is strictly valid only when the transfer integrals are much smaller than the reorganization energy. This condition is actually hardly fulfilled in a number of organic semiconductors. Recently, Brédas and coworkers theoretically demonstrated that the thermal expansion of the crystal structures, rather than the polaron formations, is the main factor responsible for the thermal bandwidth narrowing in organic semiconductors [81].

1.2.4 Trap Potentials

Most theoretical studies try to understand the intrinsic transport nature, namely, the thermally activated hopping behavior for low mobility and the power-law temperature-dependent band-like behavior for high mobility, in

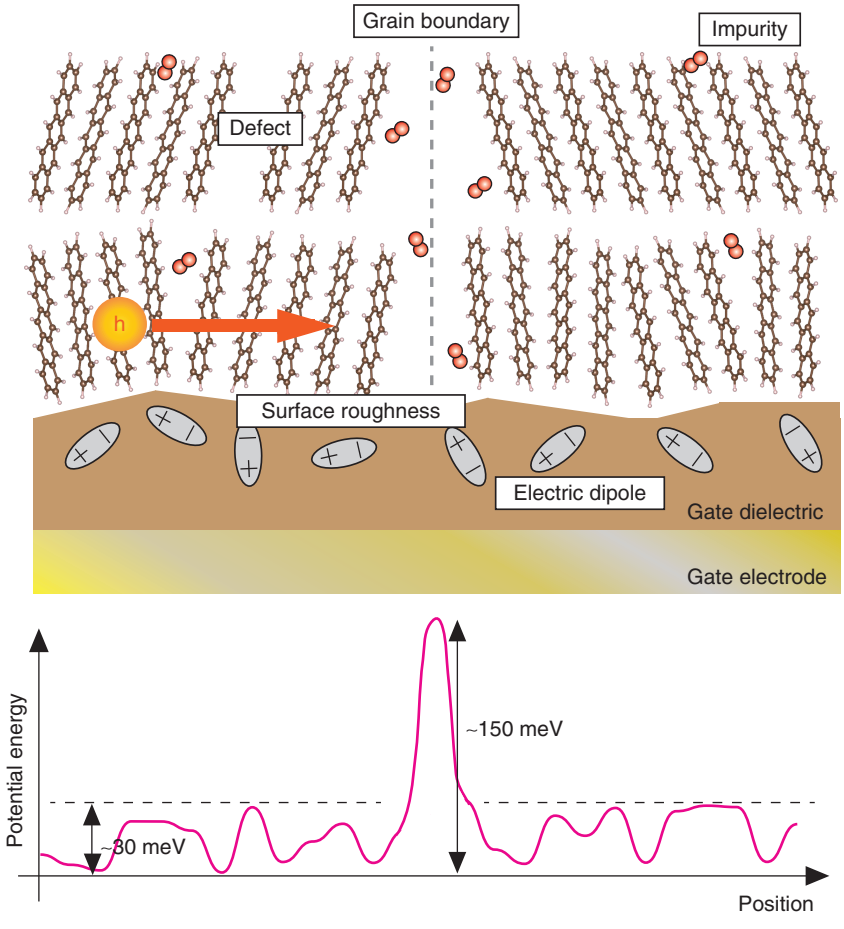

Figure 1.7 Schematic picture of various extrinsic disorders and the depth of trap potential.

organic semiconductors by taking the electron–phonon couplings into account. However, experimental data obtained on high-quality single crystals indicate that the appearance of an activated transport is in many instances more likely due to the presence of extrinsic disorder effects such as structural disorder, chemical defects [82], interaction with the substrate [57] and so on (see Figure 1.7) [70]. Such extrinsic disorders inevitably exist in actual devices and trap the carriers, resulting in decreasing the mobility. The existence of carrier-trap potentials has been confirmed by atomic force microscope potentiometry [63] and electron spin resonance spectra [83]. The depth of trap potentials W is in the range of $10–10^2$ meV, which is comparable to the magnitude of transfer integrals [84].

1.2.5 Wave-packet Dynamics Approach Based on Density Functional Theory

As discussed in Sections 1.2.1–1.2.4, the polaron concept is valid in the case of $t \ll \lambda$, whereas the band transport, where charge carriers are scattered

by phonons, is applicable in the case of $t \gg \lambda$. However, for typical organic semiconductors the transfer integrals t are in the range 10–10^2 meV, which has similar energetic orders of reorganization energy λ. Furthermore, the transfer integrals t are comparable to the depth of carrier-trap potentials W. It is important for us to understand the carrier transport mechanism in competition among the electron–phonon scatterings, the polaron formations, and the trap potentials. Especially, a unified theoretical description from the thermally activated hopping transport behavior to the band-like transport behavior represents a very challenging problem.

Therefore, I have developed the methodology named the time-dependent wave-packet diffusion (TD-WPD) method [73, 85–88], which enables us to carry out the transport calculations including the strong electron–phonon couplings and the trap potentials on equal footing without perturbative treatment. The mobility of a charge q along the x direction for an organic semiconductor with volume Ω is calculated using the following Kubo formula:

$$\mu_x = \lim_{t\to+\infty} \frac{q}{n} \int_{-\infty}^{+\infty} \mathrm{d}E \left(-\frac{\mathrm{d}f}{\mathrm{d}E}\right) \left\langle \frac{\delta(E-\hat{H}_\mathrm{e})}{\Omega} \frac{\{\hat{x}(t)-\hat{x}(0)\}^2}{t} \right\rangle, \tag{1.19}$$

where the concentration of charge carriers is obtained by $n = \int \mathrm{d}E f(E)\langle\delta(E-\hat{H}_\mathrm{e})\rangle/\Omega$. The Heisenberg picture of the position operator is defined by $\hat{x}(t) = \hat{U}^\dagger(t)\hat{x}\hat{U}(t)$, where $\hat{U}(t = N_t\Delta t) \equiv \Pi_{n=0}^{N_t-1} \exp\{i\hat{H}_\mathrm{e}(n\Delta t)\Delta t/\hbar\}$ is the time evolution operator. The dynamical change of electronic states induced by molecular vibrations and distortions is included in the time-dependent expression of Hamiltonian $\hat{H}_\mathrm{e}(t)$. The quantity $\langle\cdots\rangle$ is evaluated as $\sum_{m=1}^{N_\mathrm{wp}}\langle\Psi_m(0)|\cdots|\Psi_m(0)\rangle/N_\mathrm{wp}$, where N_wp is the number of random-phase wave-packets $|\Psi_m(0)\rangle$. Note that when the Fermi distribution function is approximated as $f(E) \simeq \mathrm{e}^{-\beta(E-E_\mathrm{F})}$, the Einstein relation $\mu_x = qD_x/k_\mathrm{B}T$ of Eq. (1.7) can be reproduced from Eq. (1.19), where the diffusion coefficient D_x is defined as $D_x \equiv \lim_{t\to+\infty}(1/t)[\int \mathrm{d}E f(E)\langle\delta(E-\hat{H}_\mathrm{e})\{\hat{x}(t)-\hat{x}(0)\}^2\rangle]/[\int \mathrm{d}E f(E)\langle\delta(E-\hat{H}_\mathrm{e})\rangle]$.

From Eqs. (1.3) and (1.5), the transfer integrals including the electron–phonon couplings are written by

$$t_{mn} = t^0_{mn} + \sum_{\lambda,\mathbf{q}} \hbar\omega_{\lambda\mathbf{q}} g^{\lambda\mathbf{q}}_{mn}(\hat{b}^\dagger_{\lambda\mathbf{q}} + \hat{b}_{\lambda-\mathbf{q}}). \tag{1.20}$$

Then, to reduce the calculation cost, I adopt the semiclassical approximation to evaluate the molecular vibrations. The phonon operators are replaced by the displacements of molecules, where the displacement of the sth molecule in the kth unit cell is defined as $\Delta\mathbf{R}_{ks} = \sum_{\lambda,\mathbf{q}} X_{\lambda\mathbf{q}} \mathbf{e}^{i\mathbf{q}\mathbf{R}_k}\mathbf{e}^{\lambda\mathbf{q}}_s$ with $X_{\lambda\mathbf{q}} = \sqrt{\hbar/2MN\omega_{\lambda\mathbf{q}}}(\hat{b}^\dagger_{\lambda\mathbf{q}} + \hat{b}_{\lambda-\mathbf{q}})$. Furthermore, I assume that the transfer integrals t_{mn} depend solely on the relative coordinate $\mathbf{R}_{mn} \equiv \mathbf{R}_m - \mathbf{R}_n$, then the semiclassical expression of transfer integrals of Eq. (1.20) is obtained as

$$t_{mn}(t) \simeq t^0_{mn} + \frac{\partial h_{mn}}{\partial \mathbf{R}_{mn}} \Delta\mathbf{R}_{mn}(t), \tag{1.21}$$

where $\Delta\mathbf{R}_{mn}(t)$ represents the change in intermolecular distance at time t due to molecular vibrations. The equation of motion for the nth molecule with mass M is

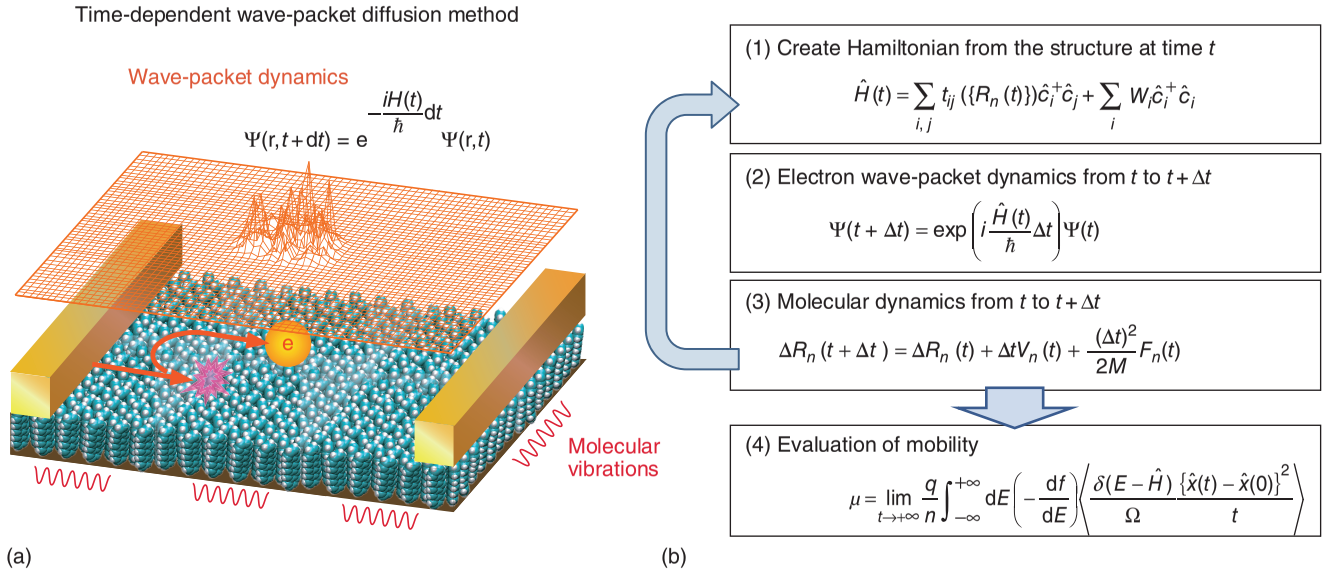

Figure 1.8 Schematic picture of an electron wave-packet propagation in the organic semiconductor (a). Flowchart of numerical calculations for evaluating the mobility using the wave-packet dynamics combined with the molecular dynamics (b).

derived from the canonical equation $M\Delta\ddot{\mathbf{R}}_n = -\partial E_{\mathrm{tot}}(\{\Delta\mathbf{R}_{ij}\})/\partial\Delta\mathbf{R}_n$, where E_{tot} is the total energy defined by the summation of electron energy and the molecular vibration energy including these interactions [87]. By extracting $\Delta\mathbf{R}_{mn}(t)$ at each time step of the molecular dynamics calculations, I can introduce the effects of strong electron–phonon couplings as the ever-changing transfer integral and obtain the mobility from Eq. (1.19). Flowchart of numerical calculations for evaluating the mobility using the wave-packet dynamics combined with the molecular dynamics and the schematic picture are shown in Figure 1.8 [70].

To reduce the computational cost, I employ the Chebyshev polynomial expansion of the time evolution operator [85, 89],

$$e^{i\frac{\hat{H}_e(t)}{\hbar}\Delta t} = \sum_{n=0}^{+\infty} e^{-i\frac{a\Delta t}{\hbar}} h_n i^n J_n\left(-\frac{b\Delta t}{\hbar}\right) T_n\left(\frac{\hat{H}_e(t)-a}{b}\right), \tag{1.22}$$

where the HOMO band is included within the energy interval $[a-b, a+b]$, and $h_0 = 1$ and $h_n = 2$ $(n \geq 1)$. The Chebyshev polynomials obey the following recursive relation: $T_{n+1}(x) = 2xT_n(x) - T_{n-1}(x)$ with $T_0(x) = 1$ and $T_1(x) = x$. As a result, the approach enables us to perform the order-N computation. Figure 1.9 shows the computing time and memory usage as a function of the number of molecules N. I confirm that the order-N calculations with respect to both the computing time and the memory usage are realized for the system of up to 10^8 molecules. The maximum system size corresponds to the two-dimensional monolayer organic semiconductor with each side length of a few micro meters. This shows that I can directly compare the transport properties calculated from atomistic treatments with the experimentally observed one.

Using the dimer approach [90, 91], I evaluate the transfer integrals t, the elastic constants K, and the electron–phonon couplings $(\partial t/\partial\Delta\mathbf{R})$ from the DFT

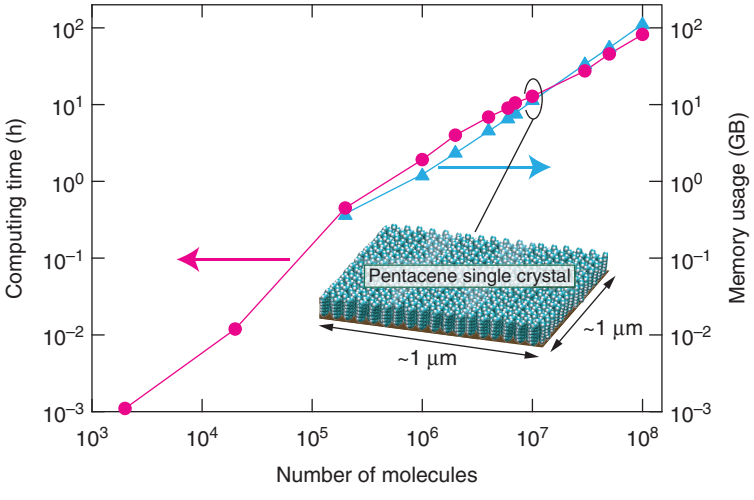

Figure 1.9 Computing time and memory usage per one wave-packet as a function of number of molecules on the TD-WPD method. The number of molecule of two-dimensional monolayer pentacene single crystal with each side length of 1 μm is shown as an example. The number of time step is set to 1000.

calculations [92] including the van der Waals interactions at the DFT-D level [93] with the Becke three-parameter Lee–Yang–Parr (B3LYP) functional in conjunction with the 6-31G(d) basis set. The all material parameters can be obtained from the DFT calculations, and the TD-WPD method enables us to evaluate the mobility of any organic semiconductors without fitting parameters.

1.3 Charge Transport Properties of Organic Semiconductors

1.3.1 Comparison of Polaron Formation Energy with Dynamic Disorder of Transfer Integrals due to Molecular Vibrations

First, the polaron formation energy of pentacene single crystal was investigated. For the simplicity, the one-dimensional crystal was employed [87]. The polaron state is obtained by self-consistent calculations to minimize the total energy E_{tot} with respect to the molecular displacements $\Delta\mathbf{R}$, namely, $\partial E_{\mathrm{tot}}/\partial\Delta\mathbf{R} = 0$ [94, 95]. When evaluating the reorganization energy used in the Marcus theory, one assumes the small polaron, thus the calculation is done for an isolated single molecule in general. As shown in Figure 1.10a, the evaluated binding energy of small polaron is 93 meV, which is enough larger than the thermal energy at room temperature [70]. However, there exist large transfer integrals of a few 10 meV between molecules in the organic semiconductor. It is considered that the polaron state is spatially extended over the crystal. Therefore, the binding energy of polaron state in the crystal having transfer integrals of 75 meV was calculated. The polaron binding energy decreases to only 14 meV, which indicates that the polaron is unstable in the crystal around room temperature.

Then, the dynamic disorder of the transfer integrals, induced by the molecular vibrations, was investigated. Figure 1.10b shows the time-dependent transfer integrals $t_{mn}(t)$ defined by Eq. (1.21) for several intermolecular bonds at 300 K

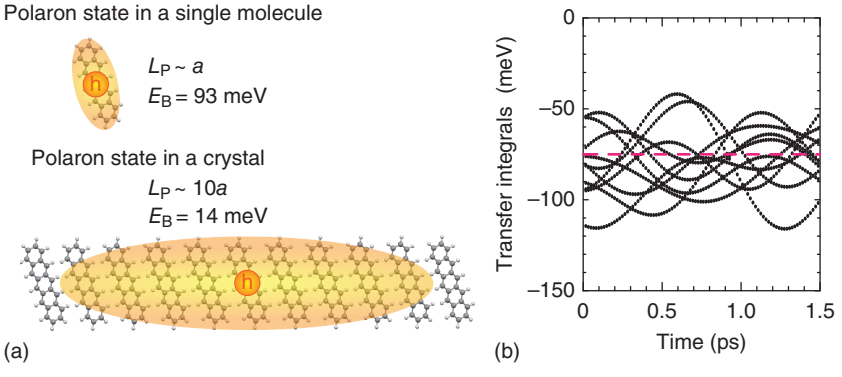

Figure 1.10 (a) Schematic picture of a polaron state in an isolated pentacene molecule and in a pentacene single crystal. The calculated binding energies of polaron state and their size are also shown. (b) Fluctuation of some transfer integrals between molecules induced by the intermolecular vibrations.

[70]. The transfer integral without any molecular vibration t^0_{mn} is 75 meV and shown by the red dashed line for comparison. The amplitude of the thermally fluctuating transfer integrals corresponding to the second term of Eq. (1.21) reaches 80 meV, which is comparable with t^0_{mn}. This calculated result indicates that the electron–phonon scattering cannot be treated by the perturbation theory such as band transport theory discussed in Section 1.2.2. Furthermore, it can be concluded that the polaron state with the binding energy 14 meV is completely destroyed by the strong dynamic disorder of transfer integrals.

1.3.2 Temperature Dependence of Mobility

Before discussing extrinsic effects of trap potentials on the charge transport, the intrinsic transport of organic semiconductors without the trap potential will be investigated. Figure 1.11a shows the logarithmic plot of mobility μ as a function of temperature [70]. As shown by the white circles, the calculated mobility μ decreases monotonically with increasing temperature approximately by the power-law dependence, which shows apparent evidence of the band-like transport. Similar power-law dependence has been reported in other theoretical works [96, 97]. The mean free path is one of the important quantities to understand the transport mechanism, since if the mean free path is shorter than the intermolecular distance, then the concept of band transport is break down. The mean free path defined by $l_{\mathrm{mfp}} \equiv v_x\tau$ can be obtained as $l_{\mathrm{mfp}} \equiv \lim_{t\to+\infty} D_x(t)/v_x$ in the TD-WPD formalism. White circles in Figure 1.11b show that the calculated mean free path is approximately 10 times longer than the intermolecular distance at room temperature [70]. It supports that the band-like transport can be realized when the trap potential is absent. However, the ideal coherent band transport is not realized in organic semiconductors because the HOMO band-edge states are spatially localized owing to the strong electron-phonon scatterings [96–99].

Next, how the mobilities are affected by the extrinsic trap potentials will be investigated, which are caused by chemical impurities, defects, randomly oriented dipoles in gate dielectric, and so on. To take the trap potentials into account, the author introduces the Anderson-type static-disorder potentials, which modulate the on-site orbital energies randomly within the energy width $[-W/2, +W/2]$ as shown in Figure 1.11c [70]. Some experiments show that the depth of trap potentials are estimated as about 50 meV [84]; thus, W is changed from 50 to 200 meV in this study. By the introduction of the trap potentials W, the magnitude of mobility is significantly decreased from 10^2 to 10^{-1} cm^2 V^{-1} s^{-1}. Furthermore, the author obtained a change in the temperature dependence from power-law dependence to thermally activated behavior via temperature-independent behavior. This behavior is experimentally observed in pentacene and rubrene devices [26, 27, 57]. When $W = 200$ meV, the mean free path is shorter than the intermolecular distance. It implies that the concept of band transport is break down, which is consistent with the hopping transport behavior of mobility. These calculated results indicate that competition between the electron–phonon scattering and the trap potential provides important clues to understand the transport nature of organic semiconductor devices.

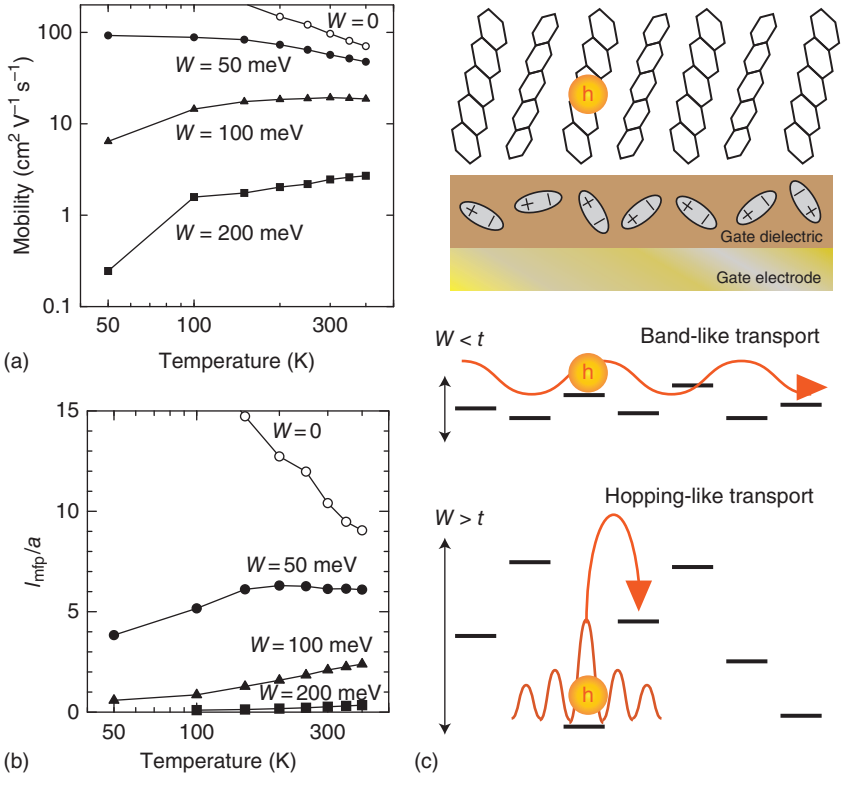

Figure 1.11 (a) Temperature dependence of mobility of pentacene single crystals for several magnitudes of trap potential W. (b) Mean free path normalized by the intermolecular distance a vs temperature characteristics for several W. (c) Schematic picture of electron (hole) transport of organic semiconductor on the gate dielectric. Randomly oriented dipoles in gate dielectric are possible origin of trap potentials. If the transfer integral t^0 is larger than the trap potential W, the electron–phonon scattering is dominated, thus the mobility decreases as increasing temperature. On the other hand, if $W > t^0$, the charge carrier is trapped tightly by the potential W; Therefore, the transport properties are close to typical thermally activated behaviors.

1.3.3 Evaluation of Intrinsic Mobilities for Various Organic Semiconductors

Finally, the author evaluated the intrinsic mobilities of representative organic semiconductors. Numerical evaluation of the intrinsic mobilities for various materials becomes a useful technique to find promising high-mobility materials suitable for organic electronics from among a number of candidate materials. Especially, the author focuses on the magnitude relation of mobilities among the various materials. As a demonstration, the TD-WPD method to the naphthalene, DNT-V, pentaene, DNTT, C_8-BTBT, and rubrene single crystals was applied. Figure 1.12b shows the mobilities obtained by the TD-WPD method. The distributions of experimentally observed mobilities in Figure 1.1g are shown by vertical bars. It can be confirmed that the calculation results well reproduce

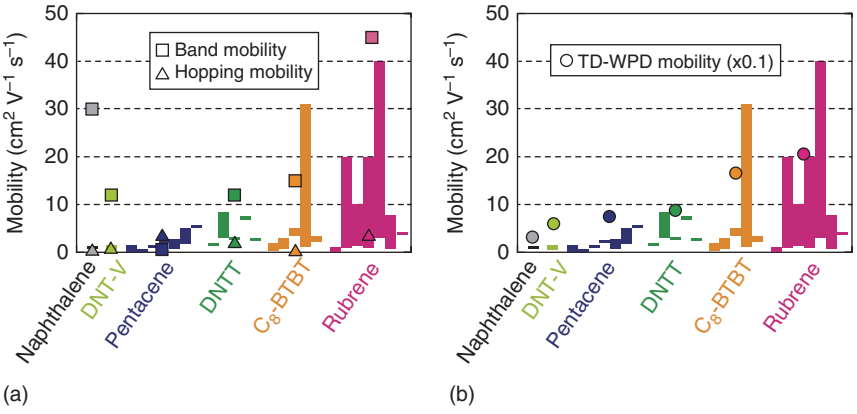

Figure 1.12 (a) Band and hopping mobilities at 300 K are plotted by squares and triangles, respectively, for naphthalene, DNT-V, pentacene, DNTT, C_8-BTBT, and rubrene. (b) Mobilities at 300 K calculated by TD-WPD method for naphthalene, DNT-V, pentacene, DNTT, C_8-BTBT, and rubrene. Note that the mobility divided by 10 for the results of TD-WPD method was plotted. Here, same material parameters, such as the transfer integrals, are employed even in above different theories. For comparison, the distributions of mobilities observed at room temperature are drawn by vertical bars.

the magnitude relation of experimentally observed mobilities for these materials. Note that the mobility divided by 10 for the results of TD-WPD method was plotted, since the wave-packet approach overestimates the magnitude of intrinsic mobility. The possible origin of the overestimation is suggested in some papers [99, 100], but still under consideration. For comparison, the band and hopping mobilities are shown in Figure 1.12a. The band and hopping mobilities cannot reproduce the magnitude relation of mobilities for some materials discussed here. For example, although the C_8-BTBT exhibits high mobility in experiments, the calculated hopping mobility is the lowest among the materials discussed here. The calculated band mobility of naphthalene is very high, whereas the mobility observed in experiment is quite low. In comparison with the conventional band and hopping models, the TD-WPD method is expected to become a useful tool to estimate and predict the magnitude relation of mobilities for candidate materials.

1.4 Summary

Organic semiconductors are expected to become key materials for realizing the printed electronics. New organic semiconductors with higher mobility have been strongly desired. However, in general, it requires time-consuming processes to synthesize these molecules, fabricate devices using the molecules, and evaluate the device performance. It is a very important and an urgent issue for us to establish the numerical simulation method for finding new organic

semiconductors with high mobility from among various kinds of the candidate materials. Evaluating the intrinsic charge transport properties of organic semiconductors requires a new theory that is able to describe the electron–phonon coupling using nonperturbative manner.

The author introduced some recent topics in the field of charge transport of organic semiconductors and presented the fundamental transport theories from an atomistic viewpoint. Then, the author's theoretical study using the TD-WPD method was presented, which enables us to evaluate the transport properties taking into account the electron–phonon couplings and the trap potentials on an equal footing without any perturbative treatment. Using this method, it was shown that the calculated temperature dependence of mobility of pentacene single crystal agrees well with experimentally observed characteristics. Furthermore, the calculated mobilities of representative organic semiconductors well reproduce the magnitude relation of experimentally observed mobilities. These calculated results indicate that, in comparison with the conventional band and hopping models, the TD-WPD method is expected to become a useful tool to estimate and predict the magnitude relation of mobilities for candidate materials.

1.4.1 Forthcoming Challenges in Theoretical Studies

As far as I know, the theoretical studies on the charge transport of organic semiconductors are divided into two approaches. One is the coherent transport approach based on the band transport, including my present study, and induces decreases in mobility with increasing temperature. Thermally activated behavior is seen only if the trap potentials are introduced into the crystal. Another one is the incoherent transport approach based on the Marcus theory, which induces the thermally activated behavior even if there are no trap potentials in crystals. Recently, a new incoherent transport approach based on a flexible surface hopping scheme was applied to a model Hamiltonian and showed the crossover from hopping transport at low electronic couplings to a band-like transport at high couplings [101]. The two approaches mentioned above give similar temperature dependences of mobility, but the physical origins are considerably different from each other. Systematic understanding of these different approaches remains an important issue.

When we try to predict the transport properties of new organic semiconductors, the precise crystal structure is the required information. Therefore, the theoretical prediction of packing structure of molecular crystal is very important. But it is known as a difficult problem in general because there exists a number of crystalline polymorphs reflecting the weak intermolecular interactions.

Furthermore, one of the main scientific challenges is to identify the microscopic origin of trap potentials in realistic organic devices. In this study, the Anderson-type static disorder potentials using W as a parameter were introduced. The inclusion of more realistic trap potentials is crucial for understanding and improving the device performance of organic semiconductors.

Acknowledgments

The author thanks K. Hirose, N. Kobayashi, J. Takeya, and S. Fratini for their valuable comments and suggestions. This work was supported by the JST-PRESTO program "Molecular technology and creation of new functions." I also acknowledge JSPS KAKENHI Grants No. 15H05418.

References

1 Wallace, P.R. (1947). *Phys. Rev.* 71: 622.
2 Eley, D.D. (1948). *Nature* 162: 819.
3 Akamatu, H. and Inokuchi, H. (1950). *J. Chem. Phys.* 18: 810.
4 Vartanyan, A.T. (1950). *Zhru. Fhim. Khim.* 24: 1361.
5 Inokuchi, H. (1954). *Bull. Chem. Soc. Jpn.* 27: 22.
6 Akamatu, H., Inokuchi, H., and Matsunaga, Y. (1954). *Nature* 173: 168.
7 Ferraris, J., Cowan, D.O., Walatka, V. Jr., and Perlstein, J.H. (1973). *J. Am. Chem. Soc.* 95: 948.
8 Shirakawa, H., Louis, E.J., MacDiarmid, A.G. et al. (1977). *J. Chem. Soc., Chem. Commun.* 578.
9 Ishiguro, T., Yamaji, K., and Saito, G. (1998). *Organic Superconductors*. Berlin, Heidelberg: Springer-Verlag.
10 Kepler, R.G. (1960). *Phys. Rev.* 119: 1226.
11 LeBlanc, O.H. (1960). *J. Chem. Phys.* 33: 626.
12 Friedman, L. (1964). *Phys. Rev.* 133: A1668.
13 Sumi, H. (1972). *J. Phys. Soc. Jpn.* 33: 327.
14 Kudo, K., Yamashita, M., and Moriizumi, T. (1984). *Jpn. J. Appl. Phys.* 23: 130.
15 Koezuka, H., Tsumura, A., and Ando, T. (1987). *Synth. Met.* 18: 699.
16 Tang, C.W. and VanSlyke, S.A. (1987). *Appl. Phys. Lett.* 51: 913.
17 Burroughes, J.H., Bradley, D.D.C., Brown, A.R. et al. (1990). *Nature* 347: 539.
18 Ohmori, Y., Uchida, M., Muro, K., and Yoshino, K. (1991). *Jpn. J. Appl. Phys.* 30: L1941.
19 Tang, C.W. (1986). *Appl. Phys. Lett.* 48: 183.
20 Xue, J., Uchida, S., Rand, B.P., and Forrest, S.R. (2004). *Appl. Phys. Lett.* 85: 5757.
21 Kim, J.Y., Lee, K., Coates, N.E. et al. (2007). *Science* 317: 222.
22 Yan, H., Chen, Z., Zheng, Y. et al. (2009). *Nature* 457: 679.
23 Rivnay, J., Jimison, L.H., Northrup, J.E. et al. (2009). *Nat. Mater.* 8: 952.
24 Karl, N. (2003). *Synth. Met.* 133–134: 649.
25 Okamoto, T., Mitsui, C., Yamagishi, M. et al. (2013). *Adv. Mater.* 25: 6392.
26 Nelson, S.F., Lin, Y.-Y., Gundlach, D.J., and Jackson, T.N. (1998). *Appl. Phys. Lett.* 72: 1854.
27 Takeya, J., Goldmann, C., Haas, S. et al. (2003). *J. Appl. Phys.* 94: 5800.
28 Butko, V.Y., Chi, X., Lang, D.V., and Ramirez, A.P. (2003). *Appl. Phys. Lett.* 83: 4773.

29 Goldmann, C., Haas, S., Krellner, C. et al. (2004). *J. Appl. Phys.* 96: 2080.
30 Roberson, L.B., Kowalik, J., Tolbert, L.M. et al. (2005). *J. Am. Chem. Soc.* 127: 3069.
31 Reese, C., Chung, W.-J., Ling, M.-M. et al. (2006). *Appl. Phys. Lett.* 89: 202108.
32 Lee, J.Y., Roth, S., and Park, Y.W. (2006). *Appl. Phys. Lett.* 88: 252106.
33 Uemura, T., Yamagishi, M., Soeda, J. et al. (2012). *Phys. Rev. B* 85: 035313.
34 Tateyama, Y., Ono, S., and Matsumoto, Y. (2012). *Appl. Phys. Lett.* 101: 083303.
35 Arabi, S.A., Dong, J., Mirza, M. et al. (2016). *Cryst. Growth Des.* 16: 2624.
36 Yamamoto, T. and Takimiya, K. (2007). *J. Am. Chem. Soc.* 129: 2224.
37 Uno, M., Tominari, Y., Yamagishi, M. et al. (2009). *Appl. Phys. Lett.* 94: 223308.
38 Haas, S., Takahashi, Y., Takimiya, K., and Hasegawa, T. (2009). *Appl. Phys. Lett.* 95: 022111.
39 Yamagishi, M., Soeda, J., Uemura, T. et al. (2010). *Phys. Rev. B* 81: 161306(R).
40 Xie, W., Willa, K., Wu, Y. et al. (2013). *Adv. Mater.* 25: 3478.
41 Kraft, U., Sejfić, M., Kang, M.J. et al. (2015). *Adv. Mater.* 27: 207.
42 Ebata, H., Izawa, T., Miyazaki, E. et al. (2007). *J. Am. Chem. Soc.* 129: 15732.
43 Izawa, T., Miyazaki, E., and Takimiya, K. (2008). *Adv. Mater.* 20: 3388.
44 Uemura, T., Hirose, Y., Uno, M. et al. (2009). *Appl. Phys. Express* 2: 111501.
45 Liu, C., Minari, T., Lu, X. et al. (2011). *Adv. Mater.* 23: 523.
46 Tanaka, H., Kozuka, M., Watanabe, S.-I. et al. (2011). *Phys. Rev. B* 84: 081306(R).
47 Soeda, J., Hirose, Y., Yamagishi, M. et al. (2011). *Adv. Mater.* 23: 3309.
48 Minemawari, H., Yamada, T., Matsui, H. et al. (2011). *Nature* 475: 364.
49 Kwon, S., Kim, J., Kim, G. et al. (2015). *Adv. Mater.* 27: 6870.
50 Podzorov, V., Pudalov, V.M., and Gershenson, M.E. (2003). *Appl. Phys. Lett.* 82: 1739.
51 Sundar, V.C., Zaumseil, J., Podzorov, V. et al. (2004). *Science* 303: 1644.
52 Stassen, A.F., de Boer, R.W.I., Iosad, N.N., and Morpurgo, A.F. (2004). *Appl. Phys. Lett.* 85: 3899.
53 Menard, E., Podzorov, V., Hur, S.-H. et al. (2004). *Adv. Mater.* 16: 2097.
54 Podzorov, V., Menard, E., Borissov, A. et al. (2004). *Phys. Rev. Lett.* 93: 086602.
55 Podzorov, V., Menard, E., Rogers, J.A., and Gershenson, M.E. (2005). *Phys. Rev. Lett.* 95: 226601.
56 Takeya, J., Tsukagoshi, K., Aoyagi, Y. et al. (2005). *Jpn. J. Appl. Phys.* 44: L1393.
57 Hulea, I.N., Fratini, S., Xie, H. et al. (2006). *Nat. Mater.* 5: 982.
58 Reese, C. and Bao, Z. (2007). *Adv. Mater.* 19: 4535.
59 Takeya, J., Kato, J., Hara, K. et al. (2007). *Phys. Rev. Lett.* 98: 196804.
60 Takeya, J., Yamagishi, M., Tominari, Y. et al. (2007). *Appl. Phys. Lett.* 90: 102120.
61 Marumoto, K., Arai, N., Goto, H. et al. (2011). *Phys. Rev. B* 83: 075302.
62 Lee, B., Chen, Y., Fu, D. et al. (2013). *Nat. Mater.* 12: 1125.

63 Ohashi, N., Tomii, H., Matsubara, R. et al. (2007). *Appl. Phys. Lett.* 91: 162105.
64 Jung, M.-C., Leyden, M.R., Nikiforov, G.O. et al. (2015). *ACS Appl. Mater. Interfaces* 7: 1833.
65 Marcus, R.A. (1956). *J. Chem. Phys.* 24: 966.
66 Hush, N.S. (1958). *J. Chem. Phys.* 28: 962.
67 Holstein, T. (1959). *Ann. Phys.* 8: 325; (1959). *Ann. Phys*. 8: 343.
68 Dimitrakopoulos, C.D. and Malenfant, P.R.L. (2002). *Adv. Mater.* 14: 99.
69 Takimiya, K., Ebata, H., Sakamoto, K. et al. (2006). *J. Am. Chem. Soc.* 128: 12604.
70 Ishii, H. (2016). *J. Inst. Elect. Eng. Jpn.* 136: 434.
71 Hannewald, K. and Bobbert, P.A. (2004). *Phys. Rev. B* 69: 075212.
72 Ortmann, F., Bechstedt, F., and Hannewald, K. (2009). *Phys. Rev. B* 79: 235206.
73 Ishii, H., Kobayashi, N., and Hirose, K. (2017). *Phys. Rev. B* 95: 035433.
74 Fukagawa, H., Yamane, H., Kataoka, T. et al. (2006). *Phys. Rev. B* 73: 245310.
75 Yamane, H., Kawabe, E., Yoshimura, D. et al. (2008). *Phys. Status Solidi B* 245: 793.
76 Koch, N., Vollmer, A., Salzmann, I. et al. (2006). *Phys. Rev. Lett.* 96: 156803.
77 Nakayama, Y., Mizuno, Y., Hikasa, M. et al. (2017). *J. Phys. Chem. Lett.* 8: 1259.
78 Northrup, J.E. (2011). *Appl. Phys. Lett.* 99: 062111.
79 Okada, Y., Sakai, K., Uemura, T. et al. (2011). *Phys. Rev. B* 84: 245308.
80 Ortmann, F., Bechstedt, F., and Hannewald, K. (2011). *Phys. Status Solidi B* 248: 511.
81 Li, Y., Coropceanu, V., and Brédas, J.-L. (2012). *J. Phys. Chem. Lett.* 3: 3325.
82 Bussolotti, F., Kera, S., Kudo, K. et al. (2013). *Phys. Rev. Lett.* 110: 267602.
83 Mishchenko, A.S., Matsui, H., and Hasegawa, T. (2012). *Phys. Rev. B* 85: 085211.
84 Kalb, W.L. and Batlogg, B. (2010). *Phys. Rev. B* 81: 035327.
85 Ishii, H., Kobayashi, N., and Hirose, K. (2008). *Appl. Phys. Express* 1: 123002.
86 Ishii, H., Kobayashi, N., and Hirose, K. (2010). *Phys. Rev. B* 82: 085435.
87 Ishii, H., Honma, K., Kobayashi, N., and Hirose, K. (2012). *Phys. Rev. B* 85: 245206.
88 Ishii, H., Tamura, H., Tsukada, M. et al. (2014). *Phys. Rev. B* 90: 155458.
89 Roche, S., Jiang, J., Triozon, F., and Saito, R. (2005). *Phys. Rev. Lett.* 95: 076803.
90 Valeev, E.F., Coropceanu, V., da Silva Filho et al. (2006). *J. Am. Chem. Soc.* 128: 9882.
91 Ishii, H., Kobayashi, N., and Hirose, K. (2013). *Phys. Rev. B* 88: 205208.
92 I used the GAMESS program at the DFT-D/B3LYP-D3/6-31G(d) level: Schmidt, M.W., Baldridge, K.K., Boatz, J.A. et al. (1993). *J. Comput. Chem.* 14: 1347.
93 Grimme, S. (2004). *J. Comput. Chem.* 25: 1463.
94 Su, W.P., Schrieffer, J.R., and Heeger, A.J. (1979). *Phys. Rev. Lett.* 42: 1698.
95 Su, W.P., Schrieffer, J.R., and Heeger, A.J. (1980). *Phys. Rev. B* 22: 2099.
96 Troisi, A. and Orlandi, G. (2006). *Phys. Rev. Lett.* 96: 086601.

97 Fratini, S. and Ciuchi, S. (2009). *Phys. Rev. Lett.* 103: 266601.
98 Picon, J.-D., Bussac, M.N., and Zuppiroli, L. (2007). *Phys. Rev. B* 75: 235106.
99 Ciuchi, S., Fratini, S., and Mayou, D. (2011). *Phys. Rev. B* 83: 081202(R).
100 Parandekar, P.V. and Tully, J.C. (2005). *J. Chem. Phys.* 122: 094102.
101 Wang, L. and Beljonne, D. (2013). *J. Phys. Chem. Lett.* 4: 1888.